Journal of Applied Fluid Mechanics, Vol. 9, No. 4, pp. 1627-1639, 2016.
Available online at www.jafmonline.net, ISSN 1735-3572, EISSN 1735-3645.

Effects of Non-Equilibrium Condensation on Deviation Angle and Performance Losses in Wet Steam Turbines

H. Bagheri Esfe, M. J. Kermani† and M. Saffar Avval

Department of Mechanical Engineering, Amirkabir University of Technology (Tehran Polytechnic), Tehran, Iran, P. Code 15875- 4413

†*Corresponding Author Email: mkermani@aut.ac.ir*

(Received April 12, 2015; accepted August 23, 2015)

ABSTRACT

In this paper, effects of non-equilibrium condensation on deviation angle and performance losses of wet stages of steam turbines are investigated. The AUSM-van Leer hybrid scheme is used to solve the two-phase turbulent transonic steam flow around a turbine rotor tip section. The dominant solver of the computational domain is the non-diffusive AUSM scheme (1993), while a smooth transition from AUSM in regions with large gradients (e.g. in and around condensation- and aerodynamic-shocks) to the diffusive scheme by van Leer (1979) guarantees a robust hybrid scheme throughout the domain. The steam is assumed to obey non-equilibrium thermodynamic model, in which abrupt formation of liquid droplets produces a condensation shock. To validate the results, the experimental data by Bakhtar *et al*. (1995) has been used. It is observed that as a result of condensation, the aerothermodymics of the flow field changes. For example for supersonic wet case with back pressure P_b=30 kPa, the deviation angle and total pressure loss coefficient change by 65% and 200%, respectively, with respect to that in dry case.

Keywords: Condensation shock; Deviation angle; Performance loss, Steam turbine.

NOMENCLATURE

a_f	speed of sound
C	chord length
c_p	specific heat capacity at constant pressure
C_P	pressure coefficient
e_t	total internal energy per unit volume
F	horizontal inviscid flux vector
F_V	horizontal viscous flux vector
G	vertical inviscid flux vector
G_V	vertical viscous flux vector
h	enthalpy
H	total enthalpy
h_{fg}	latent heat of evaporation
J	Jacobianof transformation
J_{nuc}	nucleation rate of droplets
k	turbulent kinetic energy
k_s	surface roughness
k_s^+	roughness reynolds number
k_B	boltzmann constant (=1.3807×10^{-23} J/K)
M	Mach number
m_v	mass of one molecule of water
N	total number of droplets per unit mass of mixture
p	pitch length
P	static pressure
P_0	total pressure
P_s	saturation pressure
P_b	back pressure
Q	conservative vector
r	average radius of droplets
r_c	critical radius of droplets
R_v	vapor constant
S	source term
t	time
T	temperature
T_s	saturationtemperature
u, v	velocity components
w	weighting factor
x,y	cartesian coordinates
β	inflow direction
γ	specific heat ratio of vapor
Γ	stagger angle
δ	deviation angle
Δt	time step
μ_t	turbulent viscosity
ξ	performance loss coefficient
ξ,η	curvilinear coordinates
ρ	mixture density
σ	surface tension
τ	stress tensor
ϕ	dissipation coefficient
χ	wetness fraction
ω	total pressure loss coefficient; turbulent frequency

1. INTRODUCTION

In a steam power plant, power is extracted from expanding steam in three stages namely high pressure (HP), intermediate pressure (IP) and low pressure (LP) turbines. During the expansion process in the LP turbine, the steam cools down and at some stages, droplet nucleation is occurred and a two-phase vapor-liquid mixture is appeared. Wet stages in the steam turbines are less efficient compared to those running with superheated vapor. The study of low-pressure turbine stages is of particular interest since they produce the largest portion of the power (across all of the stages), and yet are susceptible to additional losses due to the presence of a second liquid phase (Gerber and Kermani 2004). Thermodynamic irreversible losses generated with non-equilibrium conditions are significant at low-pressure stages, since the efficiency is reduced by approximately 1% for every additional percent of wetness (Baumann, 1921). On the other hand, condensation can cause some permanent damages, like mechanical erosions on the blade surface.

In the tip section of the last stages of the steam turbines, due to high velocity and excessive expansion rate of the flow, complicated phenomena could be observed. Firstly, formation of shock and expansion waves at the trailing edge can affect the behavior of the flow field. On the other hand, when the flow reaches to a specified supercooling degree, suddenly nucleates and condensation shock is formed in the supersonic flow. The condensation shock and attendance of the liquid phase can change the aerothermodynamics of the flow field in the steam turbine stages.

Researches on the low-pressure turbine stages have great importance due to widespread usage of the steam turbines for power generation. Commence of wide studies in two-phase vapor-liquid flows, backs to the 1970s when Mcdonald (1962) presented the theory of homogeneous nucleation. He studied this phenomenon in two thermodynamic and kinetic aspects.

In the next years some experimental and numerical results related to two-phase condensing flows were presented. Moore *et al*. (1973) performed one of the earliest experiments related to condensation in nozzles. Then some experiments were performed on a cascade of turbine to study the phenomena associated with spontaneous condensation by Skillings (1987, 1989). He studied the effects of inlet superheating and outlet Mach number on the trailing edge shock structure.

Bakhtar and Mahpeykar (1996) and Bakhtar *et al*. (2009) carried out some experiments to study two-phase nucleating steam flow in a blade passage. Also they performed a comparative study of the treatment of two-dimensional nucleating flows using Runge-Kutta and Denton's methods (Bakhtar *et al*. 2007).

In 1984, Young presented a theoretical investigation of chocking in steady, one dimensional, non-equilibrium wet steam in the nozzles (Young, 1984). Then he presented a method to solve the governing equations of wet steam flow in two and quasi three dimensional turbine cascades (Young, 1992). The mixture conservation equations were solved in an Eulerian reference frame and droplet phase was computed by integrating the relevant equations along true streamlines in a Lagrangian reference frame.

White and Young (1993) presented a time marching method to predict unsteady phenomena in condensing steam flows. In 2000, White developed a numerical method for the prediction of condensing steam flow within compressible boundary layers (White, 2000). Also White and Hounslow (2000) presented a new method for modeling droplet size distributions within condensing steam flows. Then White (2003) presented a comparison of modeling methods for polydispersed wet-steam flow.

In 2002, Gerber used the classical theory of nucleation and proposed a new numerical model (Eulerian-Lagrangian) to solve the two-phase compressible flows in steam nozzles and turbine blades (Gerber, 2002). Then, Gerber and Kermani (2004) presented a pressure based Eulerian–Eulerian multi-phase model for non-equilibrium condensation in transonic steam flow. In 2007, Gerber and Mousavi investigated the Quadrature Method of Moments (QMOM) in representing droplet size distributions present in the low-pressure steam turbine stages (Gerber and Mousavi 2007). Then Halama *et al*. (2010) used an in-house code for simulating two-phase condensing steam by addition of Giles's matching algorithm using Lax-Wendroff method.

Single- and two- fluid models for steam condensing flow modeling were presented by Dykas and Wroblewki (2011). In 2012, they presented the computational results of the wet steam flow through the Laval nozzles for low and high inlet pressures (Dykas and Wroblewki 2012). Also, an effective method of determination of water vapor properties was presented in the case of expansion in the nozzle at high pressures. Recently Hamidi and Kermani (2013) investigated numerical solution of a compressible two-phase moist-air flow with and without shock waves. They used the equilibrium thermodynamic model to study the condensation in a one dimensional nozzle.

According to the literature review, it can be concluded that several researches have been performed to simulate two-phase condensing flows using different numerical methods. But few researchers have investigated effects of non-equilibrium condensation on the behavior of the flow field in the wet steam turbines.

In the past, several upwind schemes have been developed and successfully used for the calculation of many problems. Prominent representatives of this class of algorithms are schemes based on the flux vector splitting and flux difference splitting concepts. Classical flux vector splitting methods are simple and very robust upwind techniques but they

exaggerate diffusive effects which take place in shear and boundary layers. On the other hand, schemes based on flux difference splitting are very accurate for viscous calculations, but at the cost of increased computational expense. Moreover, they lack robustness for flows with strong expansions into regions of low pressure and low density.

The Advection Upstream Splitting Method (AUSM) retains the robustness and efficiency of the flux vector splitting schemes but it achieves the high accuracy attributed to schemes based on the flux difference splitting concept. This method was suggested by Liou and Steffen (1993).

They used it to solve some problems (e.g. inviscid calculation of NACA 0012 airfoil, 2D supersonic flow over a circular blunt body) and compared the results with other methods (Roe, Van Leer). Based on their results, the special merits of AUSM compared to other upwind schemes are the low computational complexity and the low numerical diffusion.

The application to various relevant flow problems, however, has shown that the AUSM method has several deficiencies. It locally produces pressure oscillations in the vicinity of shocks. Furthermore, the scheme has a poor damping behavior for low Mach numbers which leads to spurious oscillations in the solution and affects the ability of scheme to capture flows aligned with the coordinate grids. In order to improve the shock resolution capability and the damping behavior of AUSM, in particular, a hybrid method was introduced by Radespiel and Kroll (1995) which switches from AUSM to the van Leer scheme at shock waves. This ensures the well-known sharp and clean shock capturing capability of the van Leer scheme and the high resolution of slip lines and contact discontinuities through AUSM. The hybrid method was used to solve some inviscid and viscous single-phase problems (e.g. calculation of RAE 2822 airfoil, flow over a compression ramp) by Radespiel and Kroll (1995). Paillere *et al*. (2003) extended the AUSM$^+$ scheme to compressible two-fluid models for gas/ liquid flow and used it to solve some two-fluid air/water flow benchmark problems from nearly incompressible flows to fully compressible flows. Niu and Lin (2006) proposed a modification of pressure-velocity diffusion terms in AUSM to compute the compressible cavitated flows based on single and two-fluid models. In the application of AUSM schemes to two-phase three-dimensional problems, we can mention the work of De Wilde *et al*. (2001) where a two-phase system composed of gas and solid particles was simulated.

In 2006, Liou extended the AUSM-family schemes to the low-Mach number limit and employed this method (AUSM$^+$-up) to solve problems at different speeds (Liou, 2006). This scheme improves over previous versions and eradicates fails found therein. Halder *et al*. (2011) used the AUSM$^+$ scheme to investigate supersonic wake of a wedge on an unstructured grid. The developed Euler solver with AUSM$^+$ flux splitting scheme was capable enough to capture the oblique shock and expansion fans properly.

Bagheri Esfe *et al*. (2015) extended the AUSM-van Leer hybrid scheme to solve the governing equations of two-phase condensing flows. The method of moments with the classical homogeneous nucleation theory was used to model the non-equilibrium condensation phenomenon.

Only few methods can correctly simulate two-phase condensing flows in a complicated geometry such as a turbine stage, because these flows experience spontaneous nucleation with sharp gradient regions. In the present paper, the AUSM-van Leer hybrid scheme is used to solvetwo-phase turbulent transonic steam flow around aturbine rotor tip section. Then, effects of condensation on different specifications of the flow field such as total pressure loss coefficient, performance loss coefficient and deviation angle are studied. Also contribution of each of the loss mechanisms such as aerodynamic-, thermodynamic- and viscous-losses from the total performance loss is determined.

It is noted that three dimensional effects could be as important as wetness effects in flows over the blades. To quantify the influences of all of these components simultaneously could be a complicated task. To isolate the influences associated with the wetness, flow in a cascade is considered here.

2. GOVERNING EQUATIONS

Assumptions using in the present study are as follows: condensation is homogenous and slip velocity between droplets and vapor is ignored due to infinitesimal radius of the droplets. Droplet-droplet and droplet-surface collisions are not taken into account in the model, because the volume occupied by the liquid phase is significantly small in comparison with the vapor phase. In fact droplet-surface collision does not have an important effect on the results.

Two-dimensional Eulerian-Eulerian governing equations for two-phase condensing flows in full conservative form are written as:

$$\frac{\partial Q}{\partial t}+\frac{\partial F}{\partial x}+\frac{\partial G}{\partial y}=S+\frac{\partial F_V}{\partial x}+\frac{\partial G_V}{\partial y} \tag{1}$$

where Q is the conservative vector, F and G are inviscid flux vectors, S is source term and F_V and G_V are viscous flux vectors which are written as follows:

$$Q=\begin{bmatrix}\rho\\ \rho u\\ \rho v\\ \rho e_t\\ \rho\chi\\ \rho N\end{bmatrix} F=\begin{bmatrix}\rho u\\ \rho u^2+P\\ \rho uv\\ \rho ue_t\\ \rho u\chi\\ \rho uN\end{bmatrix},G=\begin{bmatrix}\rho v\\ \rho uv\\ \rho v^2+P\\ \rho ve_t\\ \rho v\chi\\ \rho vN\end{bmatrix},$$

$$F_V = \begin{bmatrix} 0 \\ \tau_{xx} \\ \tau_{xy} \\ u.\tau_{xx} + v.\tau_{xy} - q_x \\ 0 \\ 0 \end{bmatrix}, G_V = \begin{bmatrix} 0 \\ \tau_{xy} \\ \tau_{yy} \\ u.\tau_{xy} + v.\tau_{yy} - q_y \\ 0 \\ 0 \end{bmatrix},$$

$$S = \begin{bmatrix} 0 \\ 0 \\ 0 \\ 0 \\ \frac{4}{3}\pi\rho_l (r_c^3 J_{nuc} + 3\rho N r^2 \frac{dr}{dt}) \\ J_{nuc} \end{bmatrix}, \quad (2)$$

where P, e_t, χ and N are pressure, total energy per unit volume, wetness fraction and total number of droplets per unit mass of mixture, respectively. In Eq. (2), J_{nuc}, r_c and $\frac{dr}{dt}$ represent nucleation rate, critical radius of droplets and radius growth rate, respectively. ρ denotes the mixture density and u, v are velocity components for both vapor and liquid. Also τ_{xx}, τ_{xy} and τ_{yy} are stress tensor components and q_x, q_y are conductive heat transfer in the horizontal and vertical directions, respectively.

Eq. (1) in generalized coordinates is written using metrics of transformation as follows:

$$\frac{\partial Q^*}{\partial t} + \frac{\partial F^*}{\partial \xi} + \frac{\partial G^*}{\partial \eta} = \frac{S}{J} + \frac{\partial F_V^*}{\partial \xi} + \frac{\partial G_V^*}{\partial \eta}, \quad (3)$$

where

$$Q^* = \frac{Q}{J}, F^* = \frac{1}{J}(\xi_x F + \xi_y G), G^* = \frac{1}{J}(\eta_x F + \eta_y G)$$
$$F_V^* = \frac{1}{J}(\xi_x F_V + \xi_y G_V), G_V^* = \frac{1}{J}(\eta_x F_V + \eta_y G_V), \quad (4)$$

where J is the jacobian of transformation and $\xi_x, \xi_y, \eta_x, \eta_y$ are the metrics of transformation. Based on the classical homogeneous nucleation theory, the number J_{nuc} of new condensed droplets per unit volume and per second is computed as (Kermani and Gerber 2003):

$$J_{nuc} = \frac{J_{cl}}{1+\varphi}, \varphi = \frac{2(\gamma-1)}{\gamma+1}\frac{h_{fg}}{R_v T_v}\left(\frac{h_{fg}}{R_v T_v} - \frac{1}{2}\right)$$
$$J_{cl} = \sqrt{\frac{2\sigma}{\pi m_v^3}} . \frac{\rho_v^2}{\rho_l} . \exp\left(-\frac{4\pi r_c^2 \sigma}{3 k_B T_v}\right),$$
$$r_c = \frac{2\sigma}{\rho_l R_v T_v \ln(P/P_S)}, \quad (5)$$

where $\gamma$is the specific heat ratio of vapor, h_{fg} equilibrium latent heat, R_v vapor constant (=461.4 J/kg.K), σsurface tension, k_B Boltzmann constant (=1.3807×10^{-23} J/K), m_v mass of one water molecule and P_s saturation pressure.

In Eq. (2), radius growth rate is obtained by (Sislian, 1975):

$$\frac{dr}{dt} = \frac{P}{h_{fg}\rho_l\sqrt{2\pi R_v T_v}} . \frac{\gamma+1}{2\gamma} . c_p . (T_l - T_v), \quad (6)$$

where

$$T_l = T_s - \frac{2\sigma T_s}{h_{fg}\rho_l r}, \quad (7)$$

T_l and T_S are droplet and saturation temperatures, respectively and c_p is specific heat capacity at constant pressure. For the present low pressure computations, the ideal gas equation of state has sufficient accuracy, hence:

$$P = \rho_v R_v T_v = (1-\chi)\rho R_v T_v . \quad (8)$$

The shear stress transport (SST) model is used to evaluate the eddy viscosity in this paper. The governing equations of this model consist of two transport equations for turbulent kinetic energy, k, and turbulent frequency, ω, and are written as follows (Menter, 1994):

$$\frac{\partial(\rho k)}{\partial t} + \frac{\partial(\rho u_j k)}{\partial x_j} = \frac{\partial}{\partial x_j}\left[(\mu_l + \sigma_k \mu_t)\frac{\partial k}{\partial x_j}\right] + P_k$$
$$- \beta^* \rho \omega k\left[1 + \alpha_1 M_t^2 (1-F_1)\right] + (1-F_1)\overline{P^{"}d^{"}}, \quad (9)$$

and

$$\frac{\partial(\rho\omega)}{\partial t} + \frac{\partial(\rho u_j \omega)}{\partial x_j} = \frac{\partial}{\partial x_j}\left[(\mu_l + \sigma_\omega \mu_t)\frac{\partial \omega}{\partial x_j}\right] +$$
$$\frac{\alpha\omega}{k}P_k + 2(1-F_1)\frac{\rho\sigma_{\omega_2}}{\omega}\frac{\partial k}{\partial x_j}\frac{\partial \omega}{\partial x_j} - \rho\beta\omega^2 \quad (10)$$
$$+ (1-F_1)\beta^* \alpha_1 M_t^2 \rho\omega^2 - \frac{\rho}{\mu_t}(1-F_1)\overline{P^{"}d^{"}},$$

where P_k being the production of turbulence. Turbulent Mach number, $M_t = \sqrt{2k/c^2}$, and pressure dilatation, $\overline{p^{"}d^{"}} = -\gamma_2 P_k M_t^2 + \gamma_3 \rho\beta^* k\omega M_t^2$, correct the compressibility effects of the flow. The coefficients of the transport equations, σ_k, σ_ω, α and β are calculated via

$$F_1 = \tanh\left\{\min\left[\max\left(\frac{\sqrt{k}}{\beta^*\omega d}, \frac{500\nu}{\omega d^2}\right), \frac{4\rho\sigma_{\omega_2}k}{CD_{k\omega}d^2}\right]\right\},$$

using the following equation:

$$\phi = F_1\phi_1 + (1-F_1)\phi_2, \quad (11)$$

which ϕ represents each of the mentioned coefficients and subscripts 1 and 2 correspond to k-ω and k-ε turbulence models, respectively. The eddy viscosity, μ_t, is evaluated using the following equation (Menter, 1994):

$$\mu_t = \frac{\alpha^* a_1 k}{\max(a_1\omega, F_2)},$$
$$F_2 = \tanh\left\{\left[\max\left(\frac{2\sqrt{k}}{\beta^*\omega d}, \frac{500\nu}{\omega d^2}\right)\right]^2\right\}. \quad (12)$$

At outlet boundary, turbulent kinetic energy k and turbulent frequency ω are extrapolated from the interior domain, whereas at inlet boundary specified free stream values of these variables are used. At walls the turbulent kinetic energy is set to zero, while turbulent frequency is computed using the relation proposed by Wilcox (2006), which includes the surface roughness:

$$\omega_w = \frac{\nu^{*2}}{\nu_\omega} S_R,$$
$$S_R = \begin{cases} 4{\lambda_R}^2 & k_s^+ \le 5 \\ \lambda_R + (4{\lambda_R}^2 - \lambda_R)e^{(5-k_s^+)} & k_s^+ > 5 \end{cases}, \quad (13)$$

where ν^* is the friction velocity, $k_s^+ = k_s\nu^*/\nu$ is the roughness Reynolds number, k_s is the roughness height and $\lambda_R = 100/k_s^+$. For the smooth walls $k_s^+ < 5$.

3. NUMERICAL DISCRETIZATION

3.1. Temporal Discretization

Using a forward Euler scheme for the time derivative, Eq. (3) is written in a semi-discrete form as:

$$\frac{1}{J}.\frac{Q^{n+1}-Q^n}{\Delta t} + \left(\frac{\partial F^*}{\partial \xi}\right)^n + \left(\frac{\partial G^*}{\partial \eta}\right)^n = \frac{S^n}{J} + \left(\frac{\partial {F_V}^*}{\partial \xi}\right)^n + \left(\frac{\partial {G_V}^*}{\partial \eta}\right)^n. \quad (14)$$

The value of Q^{n+1} is obtained from Eq. (14), then all the primitive variables $(\rho, u, v, e_t, \chi, N)$ at the new time step will be determined. Since this equation is explicit in time, stability of the solution is governed by the CFL condition (Anderson, 1995).

3.2. Spatial Discretization

Extrapolation of the primitive variables such as pressure, velocity and temperature from the cell centers to the cell faces is performed by the MUSCL strategy (Van Leer 1979). In this part, the AUSM-van Leer hybrid scheme is used to calculate the inviscid flux vectors. The underlying idea of the approach is based on the observation that the inviscid flux vectors (Eq. (2)) consist of two physically distinct parts, namely the convective and the pressure parts. The horizontal inviscid flux at the east face of the control volume is defined as (Bagheri Esfe *et al*. 2015)

$$F_{i+\frac{1}{2},j} = \frac{1}{2}.\frac{M_{i+\frac{1}{2},j}}{J}\left(\begin{bmatrix}\rho a_f\\ \rho a_f u\\ \rho a_f v\\ \rho a_f H\\ \rho a_f \chi\\ \rho a_f N\end{bmatrix}_L + \begin{bmatrix}\rho a_f\\ \rho a_f u\\ \rho a_f v\\ \rho a_f H\\ \rho a_f \chi\\ \rho a_f N\end{bmatrix}_R\right) - \frac{1}{2}.\frac{\phi_{i+\frac{1}{2},j}}{J}\left(\begin{bmatrix}\rho a_f\\ \rho a_f u\\ \rho a_f v\\ \rho a_f H\\ \rho a_f \chi\\ \rho a_f N\end{bmatrix}_R - \begin{bmatrix}\rho a_f\\ \rho a_f u\\ \rho a_f v\\ \rho a_f H\\ \rho a_f \chi\\ \rho a_f N\end{bmatrix}_L\right) + \frac{1}{J}.\begin{pmatrix}0\\ \xi_x P\\ \xi_y P\\ 0\\ 0\\ 0\end{pmatrix}_{i+\frac{1}{2},j} \quad (15)$$

The first term on the right-hand side of the above equation represents a Mach number-weighted average of the left and right states. The second term has a dissipative character. It is scaled by the scalar value $\phi_{i+\frac{1}{2},j}$ which is termed as dissipation coefficient.

The advection Mach number $M_{i+\frac{1}{2},j}$ is obtained from the relation

$$M_{i+\frac{1}{2},j} = M^+ + M^-, \quad (16)$$

where the split Mach numbers are defined by Eqs. (17) and (18),

$$M^+ = \begin{cases} M^L & for \quad M^L \ge 1 \\ \frac{1}{4}(M^L+1)^2 & for \quad |M^L| < 1 \\ 0 & for \quad M^L \le -1 \end{cases}, \quad (17)$$

and

$$M^- = \begin{cases} 0 & for \quad M^R \ge 1 \\ \frac{-1}{4}(M^R-1)^2 & for \quad |M^R| < 1 \\ M^R & for \quad M^R \le -1 \end{cases}. \quad (18)$$

The Mach numbers M^L and M^R are evaluated using the left and right states, respectively, i.e.

$$M^R = \left(\frac{U}{a_f}\right)_R, \; M^L = \left(\frac{U}{a_f}\right)_L, \quad (19)$$

Where a_f is speed of sound and evaluated from the following equation (Traupel, 1971):

$${a_f}^2 = -\frac{1}{\rho^2}.\frac{1}{(\frac{\partial \nu}{\partial P})_T + \frac{T}{c_p}(\frac{\partial \nu}{\partial T})_P{}^2},$$
$$(\frac{\partial \nu}{\partial T})_P = (1-\chi).(\frac{R}{P} + \frac{dB}{dT}),$$
$$(\frac{\partial \nu}{\partial P})_T = (\chi - 1).(\frac{TR}{P^2}),$$

$$B(T) = b_0 + \frac{b_1}{T}.\exp(\frac{b_2}{b_3 + T^2}), \quad (20)$$

$b_0 = 1.9915 \times 10^{-3}$
$b_1 = -2.21$
$b_2 = 3.0304 \times 10^5$
$b_3 = 4.3986 \times 10^4$.

The pressure at the east face of the control volume is obtained from the splitting:

$$P_{i+\frac{1}{2},j} = P^+ + P^-, \quad (21)$$

with the split pressures given by

$$P^+ = \begin{cases} P^L & for\ M^L \geq 1 \\ \frac{1}{4}.P^L.(M^L+1)^2.(2-M^L) & for\ |M^L| < 1 \\ 0 & for\ M^L \leq -1 \end{cases}, \quad (22)$$

and

$$P^- = \begin{cases} 0 & for\ M^R \geq 1 \\ \frac{1}{4}.P^R.(M^R-1)^2.(2+M^R) & for\ |M^R| < 1 \\ P^R & for\ M^R \leq -1 \end{cases}. \quad (23)$$

The dissipation coefficient in Eq. (15) is defined as sum of the dissipation terms using the van Leer and AUSM schemes:

$$\phi_{i+\frac{1}{2},j} = (1-w).\phi_{i+\frac{1}{2},j}^{VL} + w.\phi_{i+\frac{1}{2},j}^{AUSM}, \quad (24)$$

where w is the weighting factor and $\phi_{i+\frac{1}{2},j}^{VL}$ is defined as

$$\phi_{i+\frac{1}{2},j}^{VL} = \begin{cases} \left| M_{i+\frac{1}{2},j} \right| & for \left| M_{i+\frac{1}{2},j} \right| \geq 1 \\ \left| M_{i+\frac{1}{2},j} \right| + \frac{1}{2}.(M^R-1)^2 & for\ 0 \leq M_{i+\frac{1}{2},j} \leq 1 \\ \left| M_{i+\frac{1}{2},j} \right| + \frac{1}{2}.(M^L+1)^2 & for\ -1 \leq M_{i+\frac{1}{2},j} \leq 0 \end{cases}. \quad (25)$$

When the advection Mach number ($M_{i+\frac{1}{2},j}$) tends to zero, the dissipation term in Eq. (15) will approach zero, too. Thus, there will be some disturbances which cannot be damped by the scheme. In order to solve this problem, it is proposed that the scaling of the dissipation term of the AUSM method be modified as follows

$$\phi_{i+\frac{1}{2},j}^{AUSM} = \begin{cases} \left| M_{i+\frac{1}{2},j} \right| & for \left| M_{i+\frac{1}{2},j} \right| \geq \delta \\ \frac{(M_{i+\frac{1}{2},j})^2 + \delta^2}{2\delta} & for \left| M_{i+\frac{1}{2},j} \right| \leq \delta \end{cases}, \quad (26)$$

where δ is a small value $(0 \leq \delta \leq 5)$. Hence there will always be a sufficient amount of numerical dissipation. The weighting factor in Eq. (24)is defined as

$$w = \min(\upsilon_{i,j}, \upsilon_{i+1,j}),$$
$$\upsilon_{i+1,j} = \max(1 - \alpha \left| \frac{P_{i-1,j} - 2P_{i,j} + P_{i+1,j}}{P_{i-1,j} + 2P_{i,j} + P_{i+1,j}} \right|, 0), \quad (27)$$
$\alpha = 5.$

Thus according to Eqs. (24), (27), it can be seen that the hybrid method switches to the van Leer scheme at shocks and high gradient regions.

3.3. Solution Algorithm

The sequence of operations to solve two-phase Eulerian-Eulerian flow fields are listed here:

1. Initialize the problem with specified values for the primitive variables (*P, T, u, v, χ, N*),
2. Determine the conservative vector (*Q*) from Eq. (2),
3. Calculate the inviscid flux vectors for the vapor and liquid phases using Eqs. (15)-(27),
4. Calculate the viscous flux vectors using Eqs. (2) and (4),
5. Obtain the updated value of the conservative vector Q^{n+1} from Eq. (14),
6. Determine the new values of the primitive variables,
7. Implement the boundary conditions,
8. Obtain the value of residual and check for convergence,
9. If the solution is converged go to the next step, otherwise go to step 2,
10. Plot the required contours and diagrams,
11. Stop.

4. RESULTS

The geometry under study is a rotor tip section of a steam turbine, taken from Bakhtar *et al*. 1995. Fig. 1 shows this geometry and computational domain between blades. The blade section has a large stagger angle (Γ) equal to 63.27°. The chord length of the blade section (p) is 42.6 mm. Also, the inlet flow angle (β) is 38°. Moreover, inflow stagnation pressure and temperature are set to 99 kPa and 382 K, respectively. As shown in Fig. 2, size of the grid is specified as 498×65 after grid-independency test. This grid is used for numerical simulation and illustrated in Fig. 3with the close-up near the leading and trailing edges.

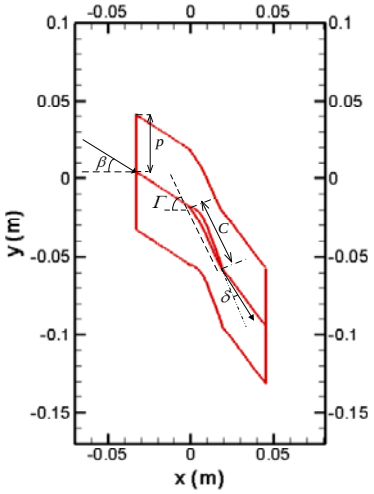

Fig. 1. Geometry of rotor-tip section and computational domain (Bakhtar *et al.* 1995); where *p* is pitch length, *C* is chord length β is flow angle at entrance, Γ is stagger angle and δ is deviation angle.

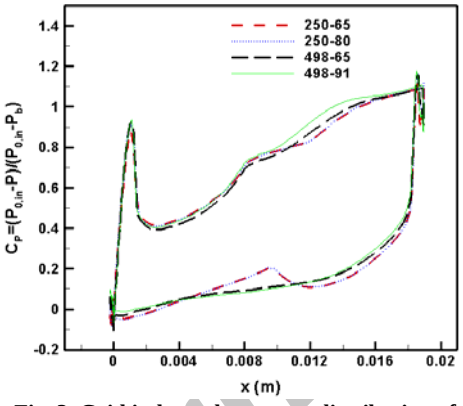

Fig. 2. Grid independency test; distribution of pressure coefficient (C_P) on the blade surface.

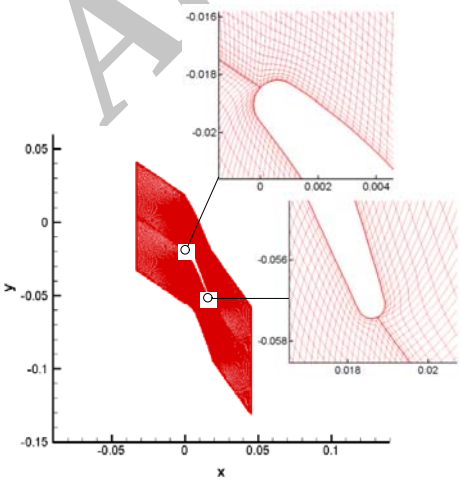

Fig. 3. Grid used for numerical simulation (498×65) with the close-up near the leading and trailing edges.

4.1. Validation

To validate the present in-house code, the numerical results of the cascade flow are compared with the experimental data of Bakhtar *et al.* (1995). The boundary conditions for the current numerical simulation have been chosen identical to those in the experimental test such as, the inflow direction is -38˚ with respect to horizontal axis, the inflow stagnation pressure and temperature are set to 99.9 kPa and 360.8 K, respectively. At the inlet section, the wetness fraction χ=0 and at the outlet section, the back pressure P_b=42.7 kPa. Comparison of the pressure ratio on the suction and pressure surfaces between numerical and experimental results is shown in Fig. 4. As observed in this figure, a good agreement between the results is obtained and the condensation shock on the suction surface is captured well.

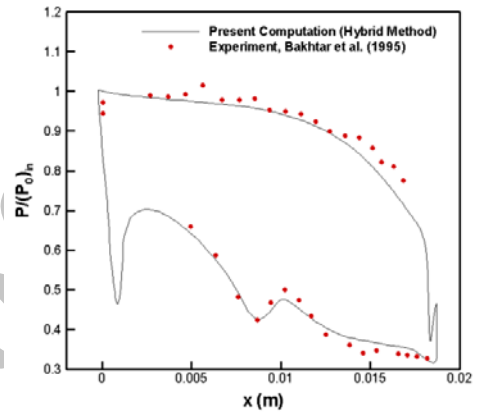

Fig. 4. Validation; comparison between numerical and experimental results (Bakhtar *et al.* 1995); Distribution of pressure ratio on the pressure and suction surfaces for the conditions $(P_0)_{in}$=99.9 kPa, $(T_0)_{in}$=360.8 K, P_b=42.7 kPa. The present computation is performed with grid size 498×65.

4.2. Effects of Outlet Pressure Variations on the Flow Field

Fig. 5 presents Mach number and wetness fraction contours in the passage for different outlet pressures. The outflow regime is supersonic for P_b=30, 45 kPa and subsonic for P_b=60 kPa. As shown in Fig. 5 (a), an oblique shock is formed at the trailing edge of the blade to match the outlet pressure in supersonic outflow cases. It is observed in Fig. 5 (b) that the wetness fraction increases with the outlet pressure reduction. For example, the outlet wetness fraction increases by 223% when the outlet pressure decreases from 60 kPa to 30 kPa. Also the wetness fraction decreases across the oblique shock due to increase in vapor temperature. Sequences of condensation and evaporation phenomena over the suction side of the blade in wet cases are shown in Fig. 5 (b).

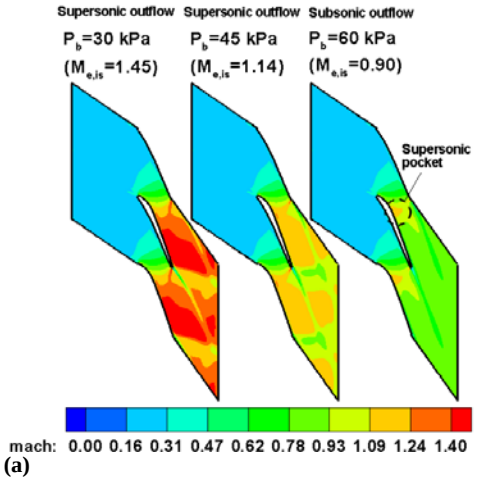

Fig. 5. Comparison of contours in the passage for different outlet pressures, (a) Mach number contours, (b) Wetness fraction contours; $(P_0)_i$=99 kPa, $(T_0)_i$=382 K.

Fig. 6 presents distribution of wetness fraction over the suction side of the blade for two different back-pressures. As observed in this figure for P_b=60 kPa, the value of wetness fraction on the suction side is almost equal to zero. Because there is lower expansion rate in comparison to the other case (P_b=30 kPa). Also wetness fraction decreases across the oblique shock near the trailing edge for P_b=30 kPa. There is no droplet formation on the pressure side as observed in Fig. 5 (b).

4.3. Effects of Condensation on Different Specifications of the Flow Field

In this part, effects of condensation on different specifications of the flow field (total pressure loss coefficient ω, performance loss coefficient ξ and deviation angle δ) are studied for smooth blades. Also contribution of each portion of loss mechanisms (aerodynamic, viscous and thermodynamic) from the total performance loss is specified. ω and ξ are computed using the following equations:

$$\omega = \frac{\Delta P_0}{P_{0_i} - P_e} = \frac{P_{0_i} - P_{0_e}}{P_{0_i} - P_e}, \tag{28}$$

and

$$\xi = \frac{h_e - h_{e,is}}{h_{0_i} - h_{e,is}} = 1 - \frac{V_e^2}{V_{e,is}^2}, \tag{29}$$

where subscripts "*i*", "*e*" and "*is*" indicate to inlet section, exit section and isentropic state, respectively.

Also deviation angle δshows the difference between flow angle and angle of camber line in the trailing edge, as depicted in Fig. 1. It is caused by the difference in the stagnation pressure between the suction and pressure surfaces around the trailing edge.

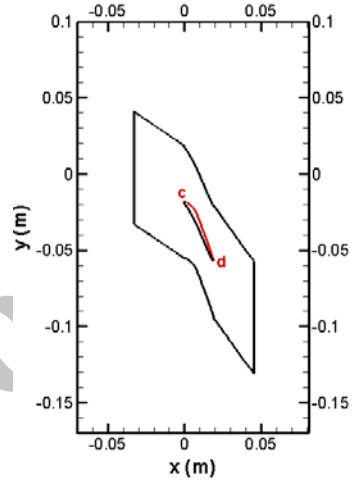

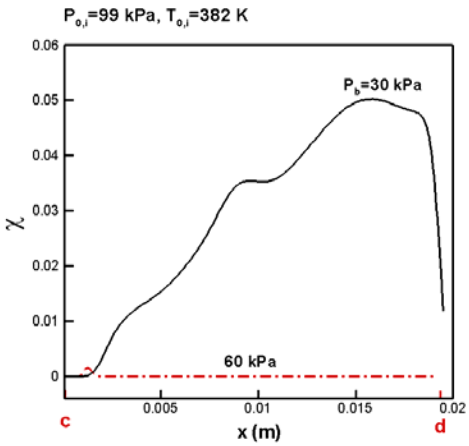

Fig. 6. Distribution of wetness fraction χ over the suction side of the blade (curve cd) for back-pressures 30 and 60 kPa.

For better understanding of the deviation angle, we consider two separate streamlines near the blade surface (Fig. 7).

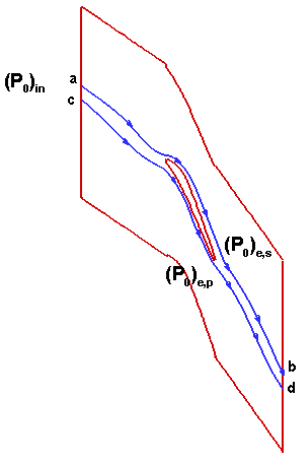

Fig. 7. Schematic representation of the streamlines near the blade surface.

As shown in this figure, the streamlines a-b and c-d pass near the suction and pressure surfaces, respectively. They have the same value of stagnation pressure at inlet boundary, namely $(P_0)_{in}$, but their stagnation pressure value differs at the trailing edge. Flow direction at the trailing edge of the blade depends on the values of $(P_0)_{e,s}$ and $(P_0)_{e,p}$ (stagnation pressure at the trailing edge near the suction and pressure surfaces).

As shown in Fig. 8 (a), flow passes tangent to the camber line at the trailing edge when $(P_0)_{e,s} = (P_0)_{e,p}$.

In the steam turbines, flow over the suction side experiences further stagnation pressure losses with respect to that of the pressure side, as it passes a sequence of condensation- and aerodynamic-shocks over the suction side, thus $(P_0)_{e,s} < (P_0)_{e,p}$. In this conditions the stream line at the trailing edge turns toward the suction surface. As depicted in Fig. 8 (b), turning of streamline at the trailing edge of the blade is called deviation angle.

Fig. 9illustrates the stream lines close to the trailing edge of blades for both dry and wet cases and two different outlet pressures. As observed in this figure, the value of deviation angle δ for supersonic outflow case (P_b=30 kPa) is more than subsonic one (P_b=60 kPa). Also wet cases have larger value of δ in comparison to dry cases.

Fig. 10 shows variation of deviation angle δ for various outlet pressures and different flow conditions of inviscid, viscous, wet and dry cases. As observed in this figure, fluid viscosity has almost no effect on deviation angle, as inviscid and viscous curves coincide on each other, and the dominant parameter in deviation angle is flow wetness or dryness. As shown in Fig. 10, δ for the wet flow is more than that in dry flow, and decreases with back pressure P_b in both wet and dry cases. Quantitatively, for P_b=30 kPa, the value of deviation angle for wet case is 65% more than that in dry case. This is due to the sequences of loss mechanisms over the suction side of blade such as condensation and evaporation phenomena in wet cases, as depicted in Fig. 5 (b). This causes excessive stagnation pressure difference between the suction and pressure surfaces that in turn increases the deviation angle in wet cases.

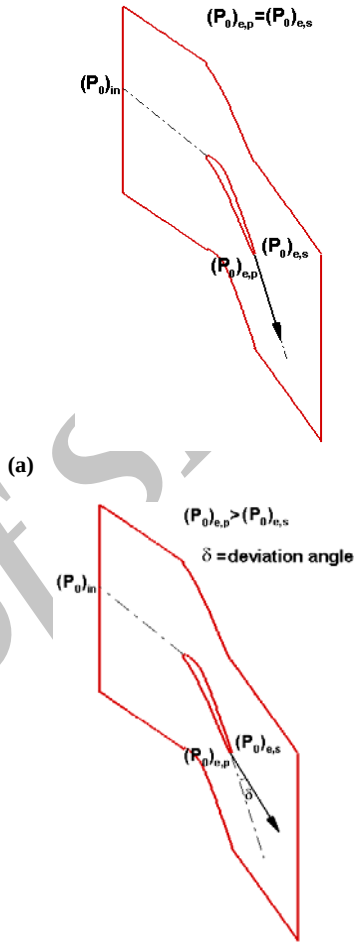

Fig. 8. Different conditions for the flow direction at the trailing edge of the blade; (a) flow passes tangent to the camber line at the trailing edge when $(P_0)_{e,s} = (P_0)_{e,p}$, (b) flow deviates at the trailing edge toward the suction side when $(P_0)_{e,s} < (P_0)_{e,p}$.

Considering the wet cases in Fig. 10, when the outlet pressure decreases from 60 kPa (subsonic outflow case) to 30 kPa (supersonic outflow condition) the deviation angle increases by 379%. This is due to increase of the wetness fraction and formation of oblique shock in the supersonic case (P_b=30 kPa). Thus supersonic outflow cases (in both wet and dry conditions) produce much larger deviation angle in comparison to subsonic ones. It is worthwhile to emphasize from practical point of view that condensation changes the deviation angle severely, hence, additional profile losses are expected in downstream of wet stages. For

example, as shown in Fig. 10, $\delta = 7.66^{\circ}$ for the wet case andP_b=30 kPa.

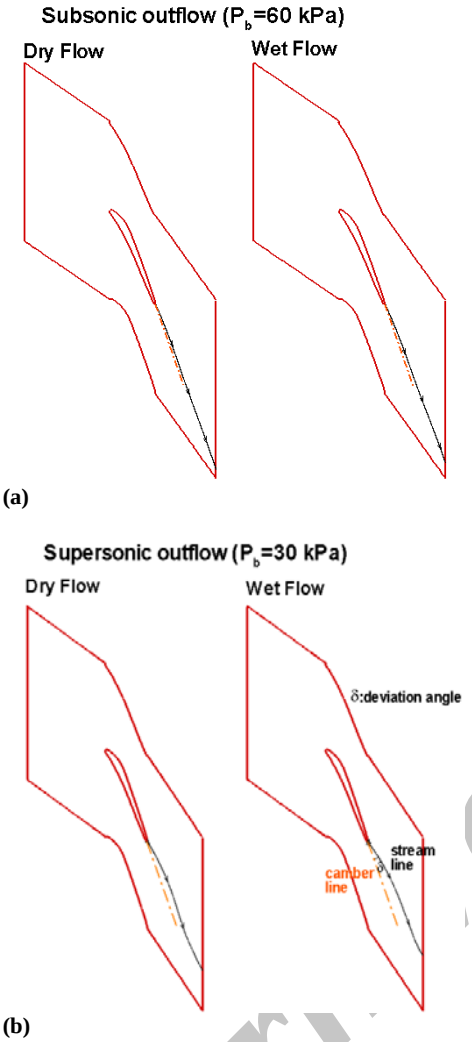

Fig. 9.Representation of the stream lines at the trailing edge of blades for dry and wet cases; (a) P_b=60 kPa, (b) P_b=30 kPa.

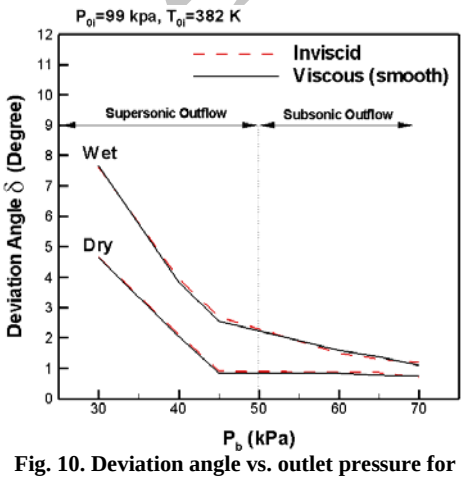

Fig. 10. Deviation angle vs. outlet pressure for different flow conditions.

Figs. 11 (a) and (b) show, respectively, values of ω and $\xi$for various outlet pressures and different flow conditions. As observed in these figures, values of ω and ξ for wet cases are much larger than those in dry flow cases. This is due to thermodynamic losses in the case of wet flows and spontaneous formation of condensation shocks in the case of supersonic outflows. For example, in viscous supersonic outflow case (P_b = 30 kPa), the values of ω and ξ for the wet flow are, respectively, 204% and 100% larger than those in dry case. Also the values of losses ω and ξ for the supersonic outflow cases are more than those in subsonic ones. This is due to the formation of aerodynamic- and condensation-shocks in supersonic outflow cases.

The prevailing feature in a non-equilibrium flow is that the temperature of the phases differs. This difference in temperature is the source of irreversible heat transfer between phases. Subsequently, the entropy generation rate throughout the flow field becomes relatively substantial and is usually referred to as thermodynamic losses. This source of loss solely exists in two-phase flow cases. Two other sources of losses (that exist in both dry and wet cases) are the aerodynamic and viscous losses.

To determine the contribution of each of the loss mechanisms from the total performance loss at a specific back pressure, we calculate the value of ξ for different flow conditions. The losses in the inviscid- dry flow are due to the aerodynamic losses of shock waves. This is shown by line segment a-b in Fig. 11 (b) for supersonic outflow regime. In subsonic flow regime the same loss is shown by line segment a′-b′. The aerodynamic loss in subsonic outflow case is due to the supersonic pocket as shown in Fig. 5 (a).

The difference in ξ between wet and dry flows (line segment b-d in Fig. 11(b)) corresponds to the thermodynamic losses in the case of supersonic outflow. Similar loss in the case of subsonic outflow is shown by line segment b′-d′ in Fig. 11 (b). The last piece of the loss is due to viscous losses in wet cases, shown by line segment d-e (for supersonic outflow case) and d′-e′ (for subsonic outflow case) in Fig. 11 (b).

Figs. 12 (a) and (b) show contribution of each of the loss mechanisms in supersonic (P_b = 30 kPa) and subsonic (P_b= 60 kPa) cases for the smooth blade. In both cases the minimum and maximum portions of the losses are due to viscous and thermodynamic losses, respectively. For smooth blades contribution of viscous losses is low in comparison to other source of losses (Moshizi *et al.* 2014).Also as observed in Fig. 12, portion of the viscous losses in subsonic outflow case (P_b = 60 kPa) is more than that in the supersonic outflow (P_b = 30 kPa). The reason is explained using Fig. 13.

Fig. 13presents ratio of the eddy viscosity to the molecular viscosity (μ_t / μ_l) .As shown in this figure, the main turbulent flow occurs in the wake region downstream of the blade. Also the value of

eddy viscosity ratio (μ_t / μ_l) in subsonic case is larger than that in supersonic outflow condition. It is also evident that the territory of turbulent region in subsonic case is bigger. As a result, larger viscous dissipation mechanisms exist in subsonic outflow condition that produce excessive losses in this case.

(a) Total pressure loss coefficient (ω)

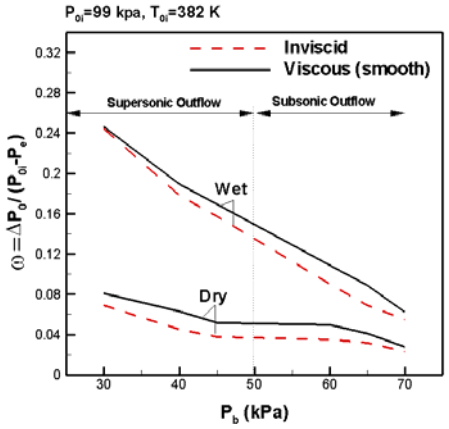

(b) Performance loss coefficient(ξ)

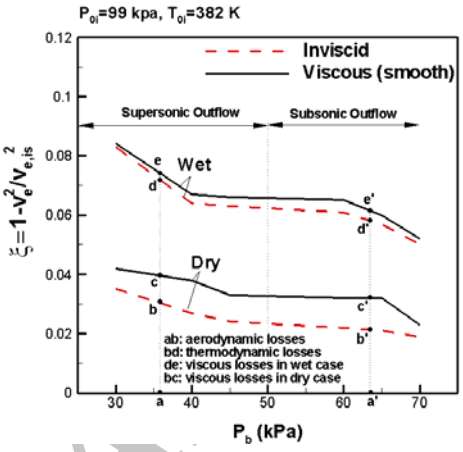

Fig. 11. Comparison of losses for wet and dry cases at different back pressures: (a) Total pressure loss coefficient ω (b) Performance loss coefficient ξ.

5. CONCLUSIONS

In this paper, the AUSM-van Leer hybrid scheme has been used to solve the transonic condensing two-phase flow around a turbine rotor tip section. The dominant solver for almost the whole domain is the non-diffusive scheme of AUSM (Liou and Steffen 1993). In regions with large gradients, e.g. in and around condensation- and aerodynamic-shocks, a smooth transition from non-diffusive AUSM scheme to the diffusive van Leer scheme guarantees a robust hybrid scheme throughout the computational domain. The eddy viscosity was determined using the SST model. According to the results obtained in this study, it is observed that:

(a)Supersonic outflow

$P_b = 30\ kPa\ (M_{e,is} = 1.45)$

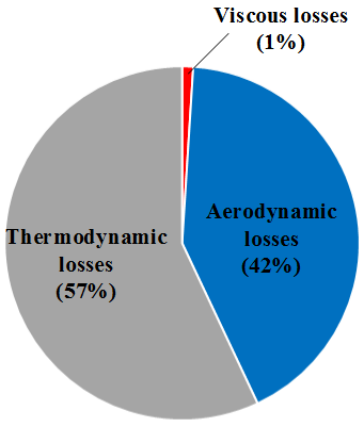

(b) Subsonic outflow

$P_b = 60\ kPa\ (M_{e,is} = 0.90)$

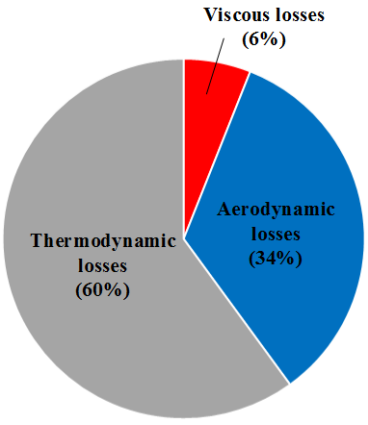

Fig. 12. Contribution of each of the loss mechanisms from ξ; Viscous wet flow passing around the smooth blade with the conditions $(P_0)_i$=99 kPa, $(T_0)_i$=382 K and (a) P_b=30 kPa, (b) P_b=60 kPa.

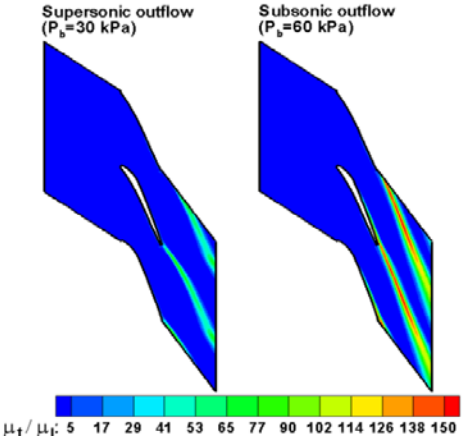

Fig. 13. Distribution of the eddy viscosity ratio (μ_t / μ_l) for wet case and two different back pressures.

- Suction surface has more expansion rate in comparison to pressure surface. Thus, condensation rate and wetness fraction near the suction side are more than those in pressure side.
- For wet cases, the values of ω, ξ and $\delta$are more than those in dry cases. This is due to condensation and released latent heat in wet cases. For example, in viscous supersonic outflow case (P_b = 30 kPa), the values of ω, ξ and δ for the wet flow are, respectively, 204%, 100% and 65% larger than those in dry case.
- The values of ω, ξ and $\delta$for supersonic outflow cases are more than those in subsonic ones. This is due to higher value of condensation rate and formation of oblique shock in the supersonic outflow cases. For example, for P_b=30 kPa (supersonic outlet) the values of ω, ξ and $\delta$are, respectively, 126%, 29% and 379% larger than those in P_b=60 kPa (subsonic outlet).
- Fluid viscosity has negligible effect on deviation angle in both subsonic and supersonic outflow cases.
- For smooth blades, either in subsonic or supersonic, and wet or dry cases, contribution of viscous losses is low in comparison to other source of losses. Hence, utilization of inviscid solvers has enough accuracy to simulate the transonic two-phase condensing flows.
- Non-equilibrium condensation has two important effects on the behavior of the flow field:

  It changes the outflow direction from its on-design condition. Thus flow entering to the next blade deviates from its on-design condition and, hence, produces additional losses. This matter should be considered in the design process of the blades located after the nucleation region in the steam turbines.

  Also, the non-equilibrium condensation increases the stagnation pressure loss and total entropy generation and decreases the turbine efficiency.

REFERENCES

Anderson, J. (1995). *Computational fluid dynamics; The basics with applications*. New York, USA: McGraw-Hill.

Bagheri Esfe, H., M. J. Kermani and M. Saffar Avval (2016). Numerical simulation of compressible two-phase condensing flows. *JAFM* 9, 3.

Bakhtar, F. and M. R. Mahpeykar (1996). On the performance of a cascade of turbine rotor tip section blading in nucleating steam, Part 3: Theoretical treatment. *Proc. IMechE, Part C: Journal of Mechanical Engineering Science* 211, 195-211.

Bakhtar, F., M. Ebrahimi and R. A. Webb (1995). On the performance of a cascade of turbine rotor tip section blading in nucleating steam, Part 1: Surface pressure distributions. *Proc. IMechE, Part C: Journal of Mechanical Engineering Science* 209, 115-124.

Bakhtar, F., M. Y. Zamri and J. M. Rodriguez-Lelis (2007). A comparative study of treatment of two-dimensional two-phase flows of steam by a Runge-Kutta and by Denton's methods. *Proc. IMechE, Part C: Journal of Mechanical Engineering Science* 221, 689-706.

Bakhtar, F., Z. A. Mamat and O. C. Jadayel (2009). On the performance of a cascade of improved turbine nozzle blades in nucleating steam. Part 2: Wake traverses. *Proc. IMechE, Part C: Journal of Mechanical Engineering Science* 223, 1915-1929.

Bakhtar, F., Z. A. Mamat and O. C. Jadayel (2009). On the performance of a cascade of improved turbine nozzle blades in nucleating steam. Part 1: Surface pressure distributions. *Proc. IMechE, Part C: Journal of Mechanical Engineering Science* 223, 1903-1914.

Baumann, K. (1921). Some recent developments in large steam turbine practice. *Journal of the Institute of Electrical Engineers* 59, 565-570.

De Wilde, J., J. Vierendeels and E. Dick (2001). An extension of the preconditioned AUSM to two-phase flows for the 3D calculation of circulating beds. *Proceedings of the Third International Symposium on Computational Technologies for Fluid/Thermal/Chemical Systems with Applications*, ASME.

Dykas, S. and W. Wroblewki (2011). Single- and two-fluid models for steam condensing flow modeling. *International Journal of Multiphase Flow* 37, 1245-1253.

Dykas, S. and W. Wroblewki (2012). Numerical modeling of steam condensing flow in low and high-pressure nozzles. *International Journal of Heat and Mass Transfer* 55, 6191-6199.

Gerber, A. G. (2002). Two-phase eulerian/lagrangian model for nucleating steam flow. *Journal of Fluids engineering* 124, 465-475.

Gerber, A. G. and A. Mousavi (2007). Application of quadrature method of moments to the polydispersed droplet spectrum in transonic steam flows with primary and secondary nucleation. *Applied Mathematical Modelling* 31, 1518–1533.

Gerber, A. G. and M. J. Kermani (2004). A pressure based Eulerian-Eulerian multi-phase model for non-equilibrium condensation in transonic steam flow. *International Journal of Heat and Mass Transfer* 47, 2217-2231.

Halama, J., F. Benkhaldoun and J. Fort (2010). Numerical modeling of two-phase transonic flow. *Mathematics and Computers in Simulation* 80, 1624-1635.

Halama, J., J. Dobe, J. Fort and K. Kozel (2010). Numerical modeling of unsteady flow in steam turbine stage. *Journal of Computational and*

Applied Mathematics 234, 2336-2341.

Halder, P., K. P. Sinhamahapatra and N. Singh (2011). Numerical investigation of supersonic wake of a wedge using AUSM$^+$ scheme on unstructured grid, *International Journal of Applied Mathematics and Mechanics* 7, 46-68.

Hamidi, S. and M. J. Kermani (2013). Numerical solution of compressible two-phase moist-air flow with shocks. *European Journal of Mechanics - B/Fluids* 42, 20-29.

Kermani, M. J. and A. G. Gerber (2003). A general formula for the evaluation of thermodynamic and aerodynamic losses in nucleating steam flow. *International Journal of Heat and Mass Transfer* 46, 3265–3278.

Liou M. S. (2006). A sequel to AUSM, Part II: AUSM$^+$-up for all speeds. *Journal of Computational Physics* 214, 137–170.

Liou, M. S. and C. Steffen (1993). A new flux splitting scheme. *Journal of Computational Physics* 107, 23-39.

Mcdonald, J. E. (1962). Homogeneous nucleating of vapor condensation I & II, Kinetic & Thermodynamic aspects. *American Journal of Physics* 30, 870-877.

Menter, F. R. (1994). Two-equation eddy-viscosity turbulence models for engineering applications. *AIAA Journal* 32, 1598-1605.

Moore, M. J., P. T. Walters and R. I. Crane (1973). Predicting the fog-drop size in wet steam turbines. *International mechanical engineering conference*, Warwick.

Moshizi, S. A., A. Madadi and M. J. Kermani (2014). Comparison of inviscid and viscous transonic flow field in VKI gas turbine blade cascade.*Alexandria Engineering Journal* 53, 275–280.

Niu, Y. and Y. Lin (2006). A robust flux splitting on simulation of transient cavitated flows based on single and two-fluid models. *European Conference on computational fluid dynamics*, Netherlands.

Paillere, H., C. Corre, and J. R. Cascales (2003). On the extension of the AUSM$^+$ scheme to compressible two-fluid models. *Computers & Fluids* 32, 891–916.

Radespiel, R. and N. Kroll (1995). Accurate Flux Vector Splitting for Shocks and Shear Layers, *Journal of Computational Physics*121, 66-78.

Sislian, J. P. (1975). Condensation of water vapor with or without a carrier gas in a shock tube. *NASA STI/Recon Technical Report N* 76, 18378.

Skillings, S. A. (1987). *An analysis of the condensation phenomena occurring in wet steam turbines*. Ph. D. thesis, CNAA, CERL.

Skillings, S. A. (1989). Condensation phenomena in a turbine blade passage. *Journal of Fluid Mechanics* 200, 409-424.

Traupel, W. (1971). *Die Grundlagen der Thermodynamik.* Karlsruhe.

Van Leer, B. (1979). Towards the ultimate conservation difference scheme, V, A second order sequel to Godunov's method. *Journal of Computational Physics* 32, 110–136.

White, A. J. (2000). Numerical investigation of condensing steam flow in boundary layers. *International Journal of Heat and Fluid Flow* 21, 727-734.

White, A. J. (2003). A comparison of modeling methods for polydispersed wet-steam flow. *International Journal for Numerical Methods in Engineering* 57, 819-834.

White, A. J. and J. B. Young (1993). Time-marching method for the prediction of two-dimensional unsteady flows of condensing steam. *Journal of Propulsion and Power* 9(2), 579-587.

White, A. J. and M. J. Hounslow (2000). Modeling droplet size distributions in polydispersed wet-steam flows. *International Journal of Heat and Mass Transfer* 43, 1873-1884.

Wilcox, D. C. (2006). *Turbulence Modeling for CFD*. 3rd edition, DCW Industries, La Canada, California.

Young, J. B. (1984). Critical conditions and the chocking mass flow rate in non-equilibrium wet steam flows. *Journal of Fluids engineering* 106, 452-458.

Young, J. B. (1992). Two-dimensional, non-equilibrium, wet-steam calculations for nozzles and turbine cascades. *Journal of Turbomachinery* 114, 569-579.